



Review

Synergistic effect from an additive induces enhanced bending resistance and self-healing properties for efficient flexible perovskite solar cells



Yue Lei, Haimin Li*, Xingchong Liu, Hanyu Wang, Huimin Dan, Yafei Ni, Wenjing Zou, Yanling Tang, Shuqian Liu, Yongshan Peng

School of New Energy and Materials, Southwest Petroleum University, Chengdu 610500, PR China

ARTICLE INFO

Keywords:
Flexible
Perovskite solar cells
Trifluorobenzenesulfonamide
Self-healing

ABSTRACT

Although more than 20% efficiency have been obtained for flexible perovskite solar cells (FPSCs), there still needs more research to essentially enhance the bending resistance and self-healing characters for flexible devices. Here, an additive of trifluorobenzenesulfonamide (TFBSA) was added into perovskite, leading to much improved bending resistance and self-healing properties. The test results demonstrate that, with synergistic effect of Lewis base, high electronegative polarity C-F group and amide group in TFBSA, the defects and carrier recombination of FPSCs are significantly inhibited, thus an excellent photoelectric conversion efficiency of 19.29% from 16.44% is obtained, and the bending resistance and self-healing nature of FPSCs are greatly improved. It can maintain 82% of its efficiency after 3000 bending cycles, while efficiency of the control decreased to 11%. At the same time, modified devices demonstrate superior self-healing properties. It is found that modified FPSC recovered from 82% to 98% of its initial efficiency when it was placed in glove box in dark at room temperature for 7 days after 3000 bending cycles. While the control one only regained 19% from 11% at same conditions. Our work provides a new strategy for FPSCs to radically enhance self-healing properties and bending resistance by adding multifunctional group additives.

1. Introduction

Since the first perovskite solar cell was introduced in 2009, it has developed rapidly in just over a decade. So far, the champion devices have achieved a photoelectric conversion efficiency (PCE) of 25.7%, showing great market potential [1]. With the development of perovskite industry chain and the satisfaction of consumer demand, wearable flexible perovskite solar cells (FPSCs) gradually appear in people's view. However, the efficiency of flexible devices is lower than that of rigid devices due to the poor quality of perovskite and lower prepared temperatures of electron transport layer [2]. Organic-inorganic hybrid perovskites usually have poor mechanical adhesion to adjacent functional layers because of their low cohesion,[3,4] and flexible substrates significantly reduce adhesion between interfaces during heat treatment due to thermal expansion/cold shrinkage. Therefore, mechanical durability and charge transfer become prominent problems affecting the efficiency of FPSCs [5,6]. And the size of bending radius and the number of bending cycles directly affect mechanical flexibility of perovskite films [7,8,41,43]. There are many reported strategies for improving

flexibility of FPSCS, such as precursor solution engineering, anti-solvent engineering[9,10] and additive engineering [11]. These methods can avoid flexural damage of FPSCs caused by stress concentration during bending, so as to improve the crystallization quality and flexibility [12,13]. For the key problem of PCE decline and irreversible recovery caused by multiple cyclic bending, some researches on self-healing methods of devices are reported. For example, organic molecules or copolymers strengthen and repair crystals to achieve self-healing [14,38]. The inherent repair properties of perovskite enable the recovery efficiency of FPSCs in dark environments [15–17]. Lan et al. reported a polyurethane elastomer with disulfide bond to achieve self-healing flexible perovskite solar cells [18]. Parisa et al. induced self-healing properties for PSCs by using PDA cations as large spacers, which can be rapidly restored after being removed from water [19]. However, self-healing perovskite is rarely reported as an effective method for device recovery.

In this work, we utilize trifluorobenzenesulfonamide (TFBSA) with multifunctional groups to prepare self-healing FPSCs. TFBSA is composed of sulfonyl, amino and halogen functional groups. When added into perovskite precursor solution, it not only plays role of

* Corresponding author.

E-mail address: lucialee@126.com (H. Li).

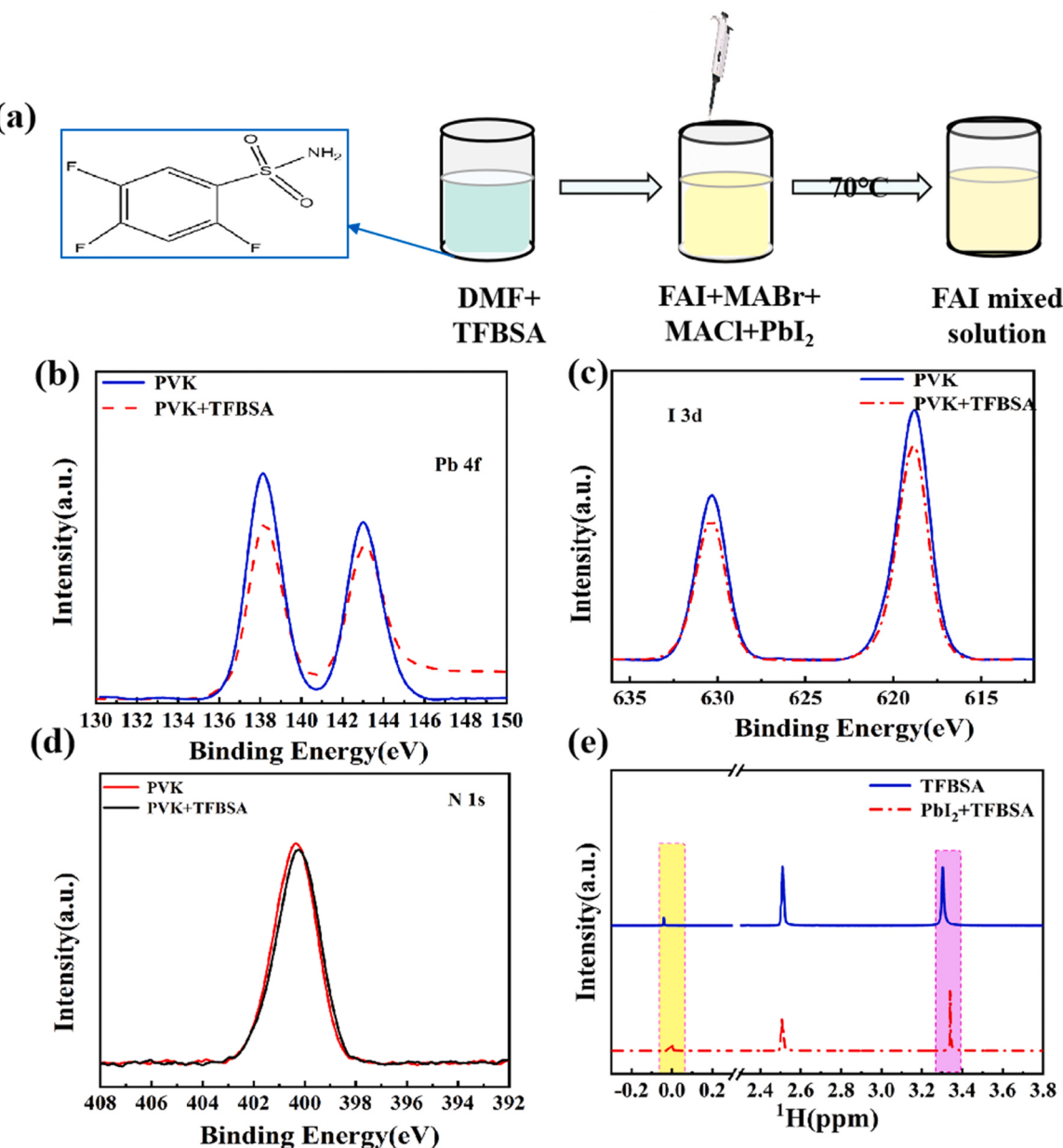


Fig. 1. (a) Chemical structure and adding process of TFBSA, (b) Pb 4 f, (c) I 3d and (d) N 1 s XPS core-level spectra of control and modified flexible perovskite film, (e) ¹H NMR spectrum of Control and TFBSA+PbI₂ solution.

passivation defects and assisting film formation, but also acts as a regulator to obtain more favorable interface bending, and forms charge transfer complex with perovskite due to its strong electron-absorbing ability [20–22]. Eventually, the efficiency of FPSCs with TFBSA modified enhanced from 16.44% to 19.29% with less hysteresis and much improved stability. After 1500 h of storage in the glovebox, it can retain 90% of its initial PCE, compared to 74% for the control one. More important, with a bending radius of 5 mm, after 3000 bending cycles, FPSCs modified by TFBSA demonstrate superior flexibility, maintaining 82% of its initial value, while the control one decreased to 11%. Notably, TFBSA can help crack perovskite films caused by bending failure (bending radius: 5 mm) to self-heal after 3000 bending cycles, which are placed in glove box under dark conditions for one week. The efficiency of modified FPSCs recovered from 82% to 98%, while the control only regained 19% from 11%. This work proves that multifunctional group additive of TFBSA can be used as a valid interface additive to promote self-healing and bending resistance for flexible perovskite devices.

2. Results and discussion

FPSCs with structure of PEN/ITO/SnO₂/Perovskite (TFBSA)/ Spiro-OMeTAD /Ag is shown in Fig. S1, in which TFBSA is directly introduced into perovskite(PVK) layer as an additive. Chemical structure of TFBSA and preparation process of TFBSA in perovskite precursor solution are shown in Fig. 1a. XPS is used to study surface chemical states of perovskite films. In perovskite film doped with TFBSA, characteristic peak of F 1 s is 687.2 eV, while there is no F 1 s peak in original one. The results demonstrate the presence of TFBSA in perovskite films (Fig. S1a). In addition, the characteristic peak of F1s of TFBSA shifted to higher binding energy in Fig. S2c, and C 1 s peak also show some deviation in Fig. S2d, indicating that there is chemical bonding between electron-rich F atom of TFBSA and electron-deficient Pb²⁺ in perovskite film, thus reducing defects on perovskite surface. Surface coordination states of Pb elements in the original and TFBSA+PVK films are in Fig. 1b. Peak of Pb 4 f_{5/2} and Pb 4 f_{7/2} are 142.9 and 138.1 eV, respectively. However, after introduction of TFBSA, binding peak of Pb 4 f moves to a higher

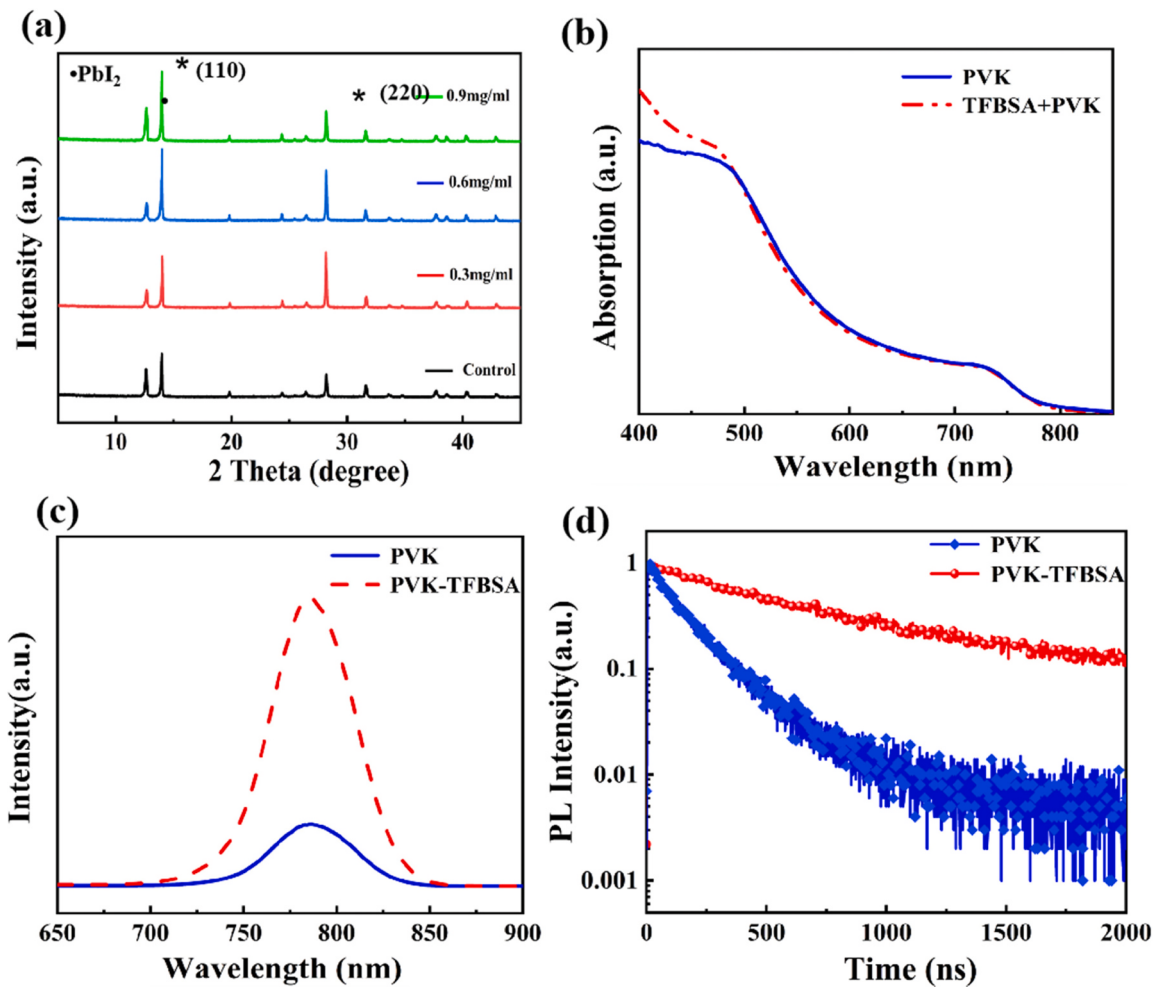


Fig. 2. (a) XRD patterns of control and PVK+TFBSA films with different concentrations, (b) UV-vis absorption spectra of control and PVK+TFBSA films, (c) Steady-state PL spectra of PEN/ITO/PVK samples and (d) TRPL patterns of perovskite for original and TFBSA-modified films.

binding energy, indicating that there is a strong interaction in perovskite film. Peak shifts are observed for I 3d and N 1 s peaks shown in Figs. 1c and 1d, which may be due to halogen atoms inhibiting vacancy formation by strengthening the chemical bonds between lead and the surrounding organic cations.[25] Meanwhile, ¹H NMR spectra of original and TFBSA+PbI₂ solution are shown in Fig. 1e. Compared with original solution of PbI₂, the proton signal of -NH₂ moved towards the direction of high chemical shift in the TFBSA + PbI₂ sample, indicating the existence of NH···I hydrogen bond interaction between TFBSA and PbI₂.[36].

In addition, interaction between TFBSA and perovskite can be further confirmed by FTIR. As shown in Fig. S2f, there are three special bonds in modified perovskite film, which are S=O bond with a peak value of 1350 cm⁻¹, C-F bond of 1060 cm⁻¹ and 1170 cm⁻¹, and C-C bond of 669 cm⁻¹ unique to TFBSA. It can be clearly observed that, compared with pure TFBSA, S=O, C-F vibrating peaks in perovskite with TFBSA shift to lower wavenumber due to chemical affinity of Pb for sulfonic acid group (SO³⁻).[23,37] Uncoordinated Pb²⁺ or Pb clusters are easy to coordinate with S, resulting in decrease of S electron cloud density. Therefore, SO³⁻ may interact with perovskite to reduce non-radiative charge recombination of perovskite, improve device performance and stability.[24].

At the same time, XPS spectra of O 1 s and S 2p (Fig. S2b and S2e) demonstrate shift for TFBSA-perovskite films, indicating that Pb²⁺ coordinates with O and S atoms in TFBSA due to that lone pair electrons of O and S atoms can fill vacant orbitals of Pb²⁺.[26] Therefore, PbI₂

deficiency is greatly inhibited after adding TFBSA, which also further confirmed the results of FTIR.

To further verify the inhibition of TFBSA on PbI₂ defects, we conducted XRD tests on the original and TFBSA modified films with different concentrations. In Fig. 2a, with 0.6 mg/ml TFBSA addition, the peak sites of perovskite (110) and (220) planes are not obviously changed while the intensity is enhanced, while relevant peak strength of PbI₂ decreased, indicating that vertical growth of perovskite crystals with TFBSA has a significant improvement.[27] Ultraviolet-visible (UV-vis) absorption spectra of the control and TFBSA-modified films are depicted in Fig. 2b. Light absorption is obviously enhanced in range of 400–500 nm. It can be confirmed that the enhancement of light absorption of TFBSA modified perovskite films can effectively speed up electron extraction from the active layer to electron transport layer, which results in larger J_{sc} for FPSCs.

To study the effect of TFBSA modification on electron extraction capability and carrier recombination, the steady-state photoluminescence (PL) characteristics of pristine and TFBSA treated perovskite films are examined.

Higher PL intensity of TFBSA-doped perovskite film shows that TFBSA can pierce shallow surface of perovskite and passivate grain boundary defects in Fig. 2c, which manifest that introduction of TFBSA can enhance charge extraction ability of perovskite and inhibit carrier recombination.[25,28] Time resolved photoluminescence (TRPL) decay is applied to quantify carrier lifetime of perovskite films in Fig. 2d. TRPL decay curve is fitted by double exponential decay function, and formula

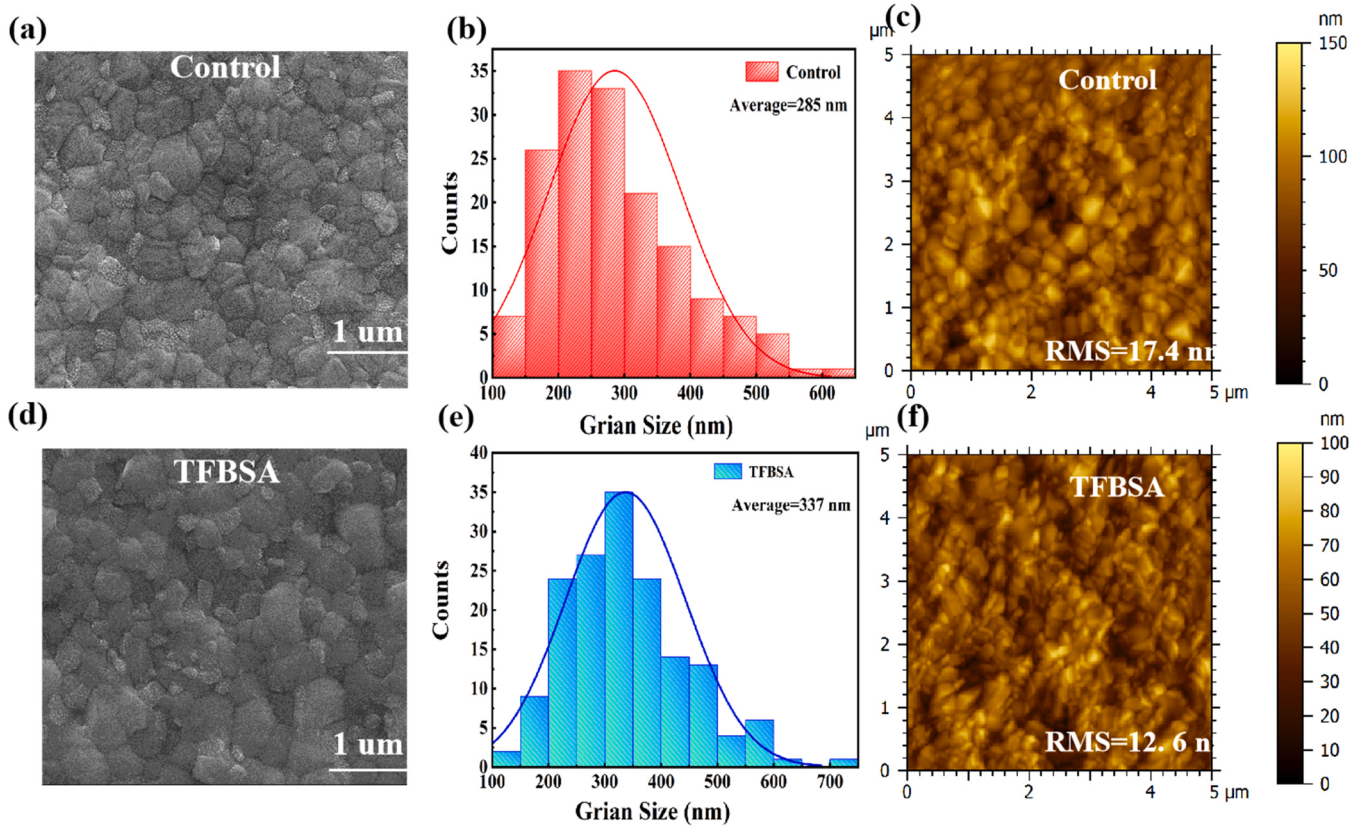


Fig. 3. SEM images of (a) control and (d) TFBSA-modified perovskite films. Distribution statistic of perovskite grain sizes of (b) control and (e) PVK+TFBSA films. AFM diagrams of perovskite film for (c) control and (f) modified TFBSA.

is as follows:

$$y = A_1 \exp(-t/\tau_1) + A_2 \exp(-t/\tau_2) \quad (1)$$

The relative amplitudes are expressed as A_1 and A_2 . τ_1 and τ_2 represent fast and slow recombination carrier lifetimes separately, which are attributed to bimolecular and trap assisted recombination of photogenic free carrier respectively.^[28] Fitting parameters summary as shown in Table S1. The average life of PL decay can be obtained by type:^[29]

$$\tau_{ave} = (A_1\tau_1^2 + A_2\tau_2^2)/(A_1\tau_1 + A_2\tau_2) \quad (2)$$

The results show that the average PL lifetime (preservation) of TFBSA-modified perovskite film is about three times of that the original one, and its value is 635.3 ns. It is confirmed that TFBSA additives can effectively enhance carrier lifetime and reduce nonradiative recombination, proving the enhancement of the quality of films.

To further investigate the role of TFBSA on the energy level of perovskite, ultraviolet photoelectron spectrometer (UPS) is employed to characterize perovskite films before and after modification. As shown in Fig. S3, Fermi edge (E_{F-edge}) and cut-off binding energy ($E_{cut-off}$) of PVK without and with TFBSA addition are 0.70 eV, 0.72 eV, and 16.17, 16.32 eV, separately. Fermi level (E_F) of the control and TFBSA-modified PVK are calculated by model $E_F = 21.22 - E_{cut-off}$ to be -5.05, -4.90 eV, separately. The valence band position (E_{VB}) of PVK without and with TFBSA addition are calculated to be -5.75, -5.62 eV, separately, which determined the conduction band position (E_{CB}) of samples as [36].

$$E_{CB} = E_g + E_{VB} \quad (3)$$

The band gap (E_g) of original and TFBSA-modified PVK are determined to be 1.56 eV after calculation of the UV absorption values of perovskite films. Therefore, PVK and PVK + TFBSA position of conduction band (E_{CB}) are 4.19, 4.06 eV, separately. As shown in Fig. S3d. It

can be seen that the doping of TFBSA makes the perovskite close to the matching energy level of hole transfer layer, which is conducive to the increase of V_{OC} .

To study the relationship between surface morphology and properties of perovskite, the surface morphology of perovskite before and after TFBSA modification is characterized by scanning electron microscopy (SEM) in Fig. 3(a and d). And the distribution statistic of perovskite grain size is shown in Fig. 3(b and e). The average grain size obtained for the original and TFBSA modified flexible perovskite film is about 285 nm and 337 nm, respectively, showing reduced boundaries, which is favorable for efficient charge transfer.^[31,32] Meanwhile, we utilize atomic force microscope (AFM) to characterize surface properties, as shown in Fig. 3(c and f). Compared with the original one, root mean square (RMS) of TFBSA-modified perovskite film decreased from 17.4 nm to 12.6 nm. Evidently, addition of TFBSA is more conducive for improving crystal quality, promoting carrier migration and reducing leakage current.

As shown in Fig. 4a, current density voltage ($J-V$) curves of the control and TFBSA doped FPSCs are depicted, and specific data are detailed in Table 1. PCE for control device is 16.44% with short-circuit current (J_{SC}) of 21.74 mA cm^{-2} , open-circuit voltage (V_{OC}) of 1.099 V, and fill factor (FF) of 68.80%, while PCE of TFBSA modified FPSCs increased to 19.29%, with a larger V_{OC} of 1.103 V, J_{SC} of 23.46 mA cm^{-2} and FF of 74.60%. TFBSA modified FPSCs reveals obviously higher V_{OC} and FF than the control one, mainly based on the reduction of defects and carrier recombination.^[30,42–44] The increased J_{SC} of TFBSA modified FPSCs is due to the enhancement of particle size and charge transportation. External quantum efficiency (EQE) spectra of two FPSCs are shown in Fig. 4b. Meanwhile, the integrated J_{SC} value from EQE is consistent with results from $J-V$ curves. As shown in Fig. 4c, stable current PCE output of the devices is further monitored at the maximum power point (MPP) bias voltage. For doped and original FPSCs, stable

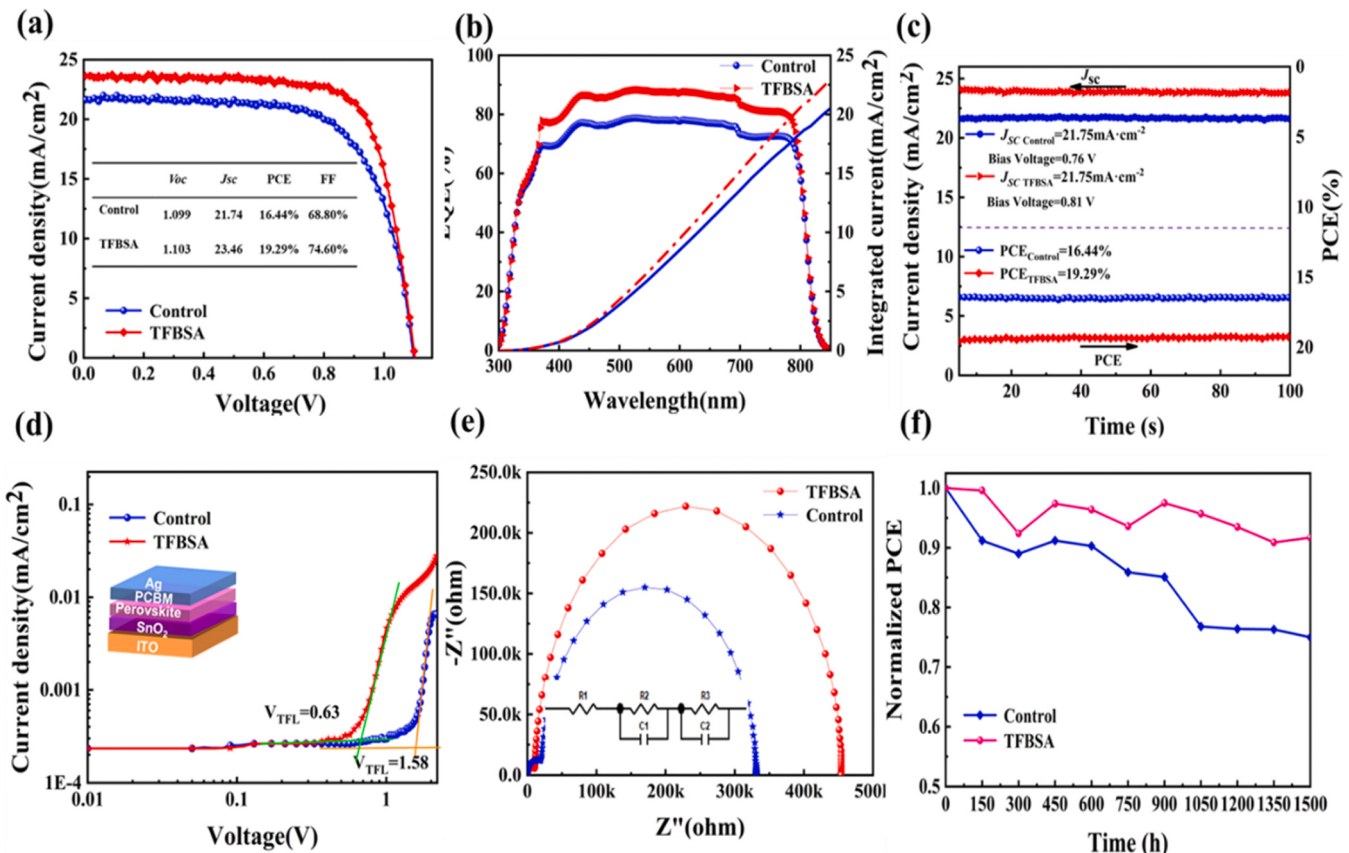


Fig. 4. (a) $J-V$ curves of the control and optimal TFBSA-doped FPSCs. (b) EQE and the corresponding integrated J_{sc} of control and optimal FPSCs, (c) Steady-state output photocurrent and PCE of control and TFBSA FPSCs at 0.8 V bias under 1 sun illumination, (d) Dark $J-V$ curves of perovskite pure electron transport layer device before and after TFBSA doped, inset illustrates the structure of the device, (e) EIS spectra of control and TFBSA-perovskite flexible devices, the inset demonstrates the equivalent circuit of the device. (f) Stability of FPSCs in a nitrogen filled glovebox in dark at room temperature.

Table 1
Best (Average) photovoltaic parameters of control and TFBSA-doped FPSCs.

Sample		V_{oc} [V]	J_{sc} [mA/cm ²]	FF [%]	PCE [%]
Control	MAX	1.099	21.74	68.80	16.44
	AVER	1.040	21.83	67.90	15.42
0.3 mg/ml	MAX	1.050	21.43	76.60	17.23
	AVER	1.050	21.50	73.30	16.47
0.6 mg/ml	MAX	1.103	23.46	74.60	19.29
	AVER	1.090	22.90	73.83	18.43
0.9 mg/ml	MAX	1.099	23.92	71.80	18.88
	AVER	1.060	22.41	70.39	16.72

PCEs are 19.29% and 16.44%, respectively. It can be seen that modified device show more stable efficiency output. To further verify repeatability of the devices, photovoltaic performance of 20 devices in each group were tested. Statistical distribution of four main parameters of control and TFBSA-doped FPSCs are shown in Fig. S4. The optimal $J-V$ characteristics of FPSCs doped with TFBSA at different concentrations have been tested, under a control sunlight intensity (1.5 AM, 100 mW cm⁻²), as shown in Table 1 and Fig. S5b. With increase of TFBSA concentration, PCE of the devices increased, and when it increased to 0.6 mg/ml, FPSC demonstrates the highest efficiency, indicating that the optimal concentration is 0.6 mg/ml.

Fig. S5a demonstrates reverse and forward $J-V$ curves for TFBSA-doped and original flexible devices. Calculation method of hysteresis index (HI) was applied. The HI decreases from 17.4% to 9.1% for original and TFBSA-doped devices.[33] This result shows that larger grain size and less defects of perovskite are the main factors for improvement

of comprehensive performance of FPSCs. The reduction of HI in TFBSA-doped devices may be due to the chemical connection between sulfonyl group and FAI.[34] Fig. 4d is the dark $J-V$ curve characteristic diagram of flexible devices with pure electronic layer structure, and the device structure illustration is shown in Fig. 4d. The V_{TFL} (trap filling limited voltage) in this figure can be used to further calculate defect density of states in TFBSA doped devices, where V_{TFL} indicates that trap state is filled by the injected carrier.[34] Its calculation formula is as follows:

$$V_{TFL} = eN_t L^2 / 2\epsilon_0 \epsilon \quad (4)$$

where e , N_t , L , ϵ_0 and ϵ represent elementary charge, trap density, thickness of perovskite film, vacuum permittivity and relative dielectric constant of the perovskite, respectively.[35] The V_{TFL} value of the control and TFBSA-doped device is 1.58 and 0.63 V, separately. Therefore, the statistical trap state density of the original and TFBSA modified flexible devices ranges from 4.954×10^{15} cm⁻³ significantly reduced to 1.976×10^{15} cm⁻³. To further study the effect of TFBSA on migration and transport in FPSCs, as shown in Fig. 4e, electrochemical impedance spectroscopy (EIS) curves of the control and TFBSA-doped device are tested under dark condition. Detailed parameters of equivalent circuit fitting are shown in Table S2 and the model is shown in Fig. 4e. The circuit model consists of a series resistor (R_1), transfer resistance (R_2), and recombination resistance (R_3).[36–40] Compared with the control one, TFBSA-doped FPSCs shows a smaller R_2 and higher R_3 . A decrease in R_2 leads to the increase of J_{sc} , indicating better carrier transport, while the increase of R_3 indicates inhibition of charge recombination,[33] which also verifies the reliability of above PL and TRPL results, thus a higher PCE is obtained. To explore the stability of FPSCs before and after

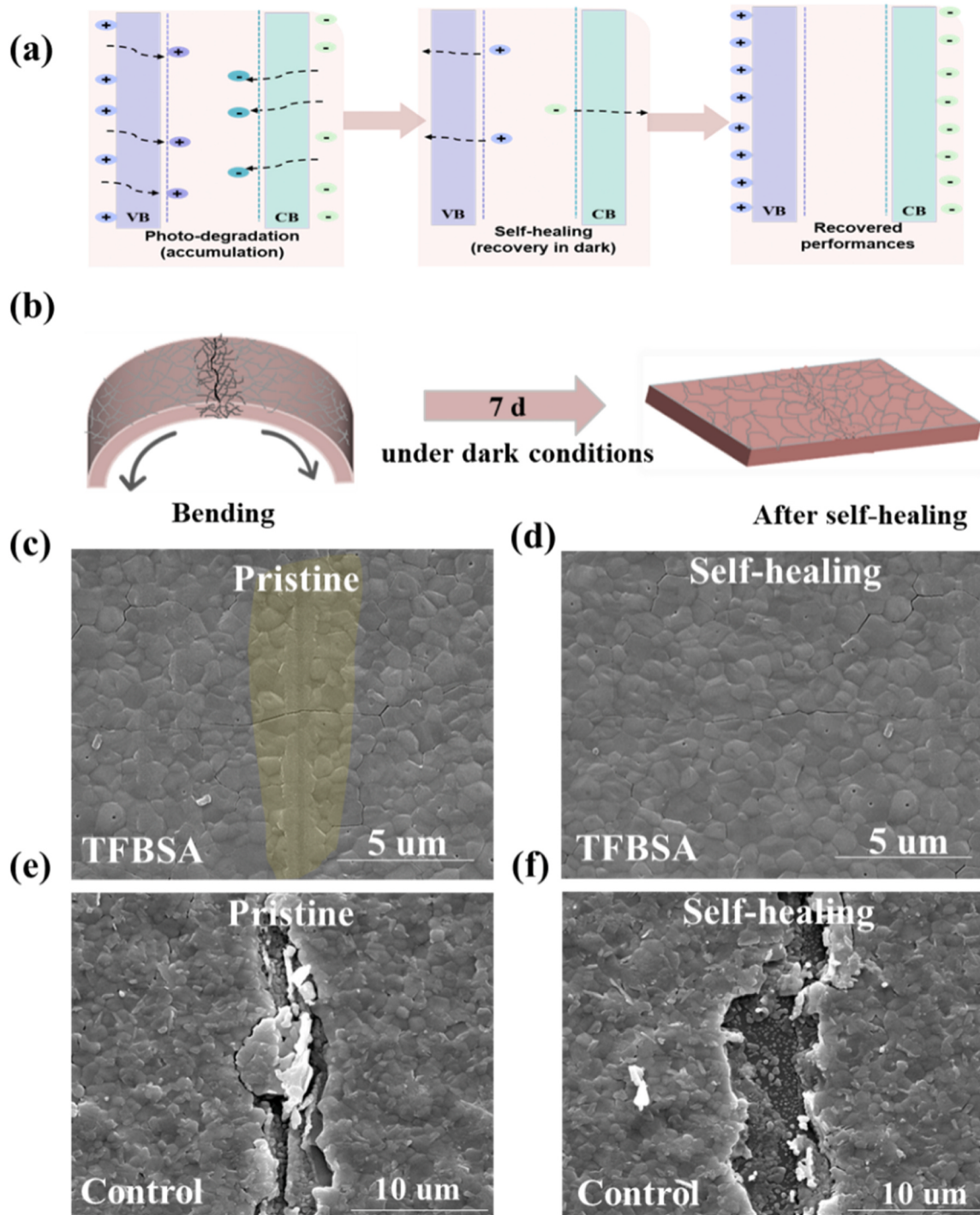


Fig. 5. (a) Evolution diagram of photocurrent degradation and self-healing mechanism of perovskite band structure,[37] (b) Schematic diagram of perovskite film with TFBSA before and after self-healing, (c) and (d) SEM of perovskite films with TFBSA before and after self-healing, (e) and (f) SEM of perovskite films before and after self-healing.

TFBSA addition, it has been tested at room temperature and in glove box filled with N_2 . It can be seen that TFBSA-doped FPSCs can retain more than 90% of its initial PCE after 1500 h in Fig. 4f. While pure FPSCs decreased to 74%, indicating that long-term stability of TFBSA doped FPSCs has been improved. At the same time, water contact angle of TFBSA-doped perovskite film increased to 53°(Fig. S6), indicating that additive of TFBSA contributes to hydrophobicity of perovskite film. This result is consistent with long-term stability of flexible device. Shockingly, under constant light for one day and then stored in glove box in darkness, the PCE of flexible devices fluctuated over time. Thus, it can be

concluded that light activates trap state, and then the FPSCs self-heals to some extent under dark conditions.[37].

Fig. 5a depicts self-healing schematic pictures of valence bands (VB) and conduction bands (CB) under light conditions after photo-degradation and recovery in darkness. The dotted line represents light activated metastable trap state, which relaxes in dark and restores device to a stable state. The arrows depict how photogenerated carriers fill light-activated trap states under light, or with the passage of time to relax in dark.[37,38,40–45] Schematic diagram of perovskite film with TFBSA before and after self-healing is shown in Fig. 5b. It can be found

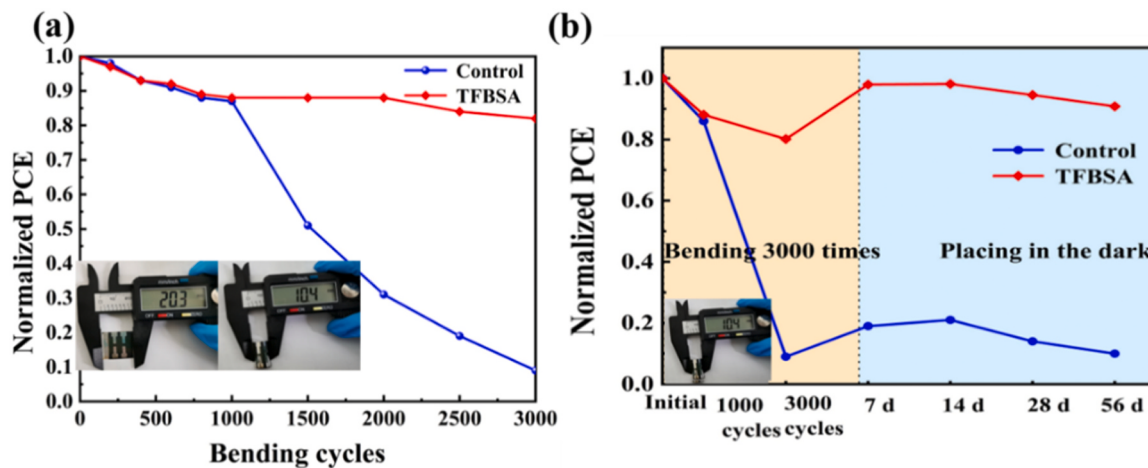


Fig. 6. (a) Bending performance results of unmodified and modified FPSCs with 5 mm bending radius, (b) Self-healing stability of devices placed in dark after bending 3000 times. The inserted images in (a) and (b) represent the values of bending radius.

from Fig. 5c and Fig. 5d that for perovskite film modified by TFBSA, the crack, resulted from bending failure for 3000 times, disappeared when it was placed under dark condition for 7 days, indicating obviously enhanced self-healing performance. While the control one shows an apparently bending trail under same circumstances (Figs. 5e and 5f), and the crack trace after 3000 bending times showed no signs of repair after 7 days in the dark. Remarkably, modified FPSCs demonstrate enhanced self-healing properties.

To verify the effect of bending on the flexibility of FPSCs, as shown in Fig. 6a, normalized PCE of FPSCs is measured after 3000 bending cycles under curvature radius of 5 mm. After 3000 bending cycles, TFBSA modified FPSC shows excellent bending resistance and can maintain 82% of its initial value, while the control one only retained 11%, which is due to greatly improved crystallization strength of perovskite crystals with introduction of TFBSA, thus enabling the perovskite films to bind together closely during the bending process.

In addition, after 3000 bending cycles, followed by 7 days in dark condition, PCE of TFBSA-modified device recovered from 82% to 98% of its original value, as shown in Fig. 6b. And after 56 days in glove box in dark, the PCE of TFBSA-modified FPSCs can still maintain more than 90% of its initial efficiency, while the original one only recovered from 11% to 19% after 7 days and it decreased to 12% after 56 days in glovebox in dark at room temperature conditions. This phenomenon directly reflects the improved self-healing ability of perovskite by TFBSA-modified FPSCs, which provides a new idea for preparation of commercial flexible perovskite solar cell devices.

3. Conclusion

In conclusion, TFBSA is successfully added into perovskite precursor solution and greatly enhanced photovoltaic performance of FPSCs. Crystallization of Modified perovskite with TFBSA are validly promoted through synergistic effect of functional groups, and trap states and carrier recombination are obviously decreased, thus greatly accelerate transfer of holes from perovskite layer to HTL, eventually, a maximum PCE increases from 16.44% to 19.29% with reduced *J-V* hysteresis and improved stability. More importantly, compared with pristine perovskite films, TFBSA-containing perovskite films have significantly improved bendability because of the compactness and high elasticity produced by TFBSA. More important, modified FPSCs demonstrate enhanced self-healing properties. After 3000 bending cycles, followed by 7 days in glove box in the dark at RT conditions, we found that PCE of TFBSA-modified device recovered from 82% to 98% of its original value, while the control one only regained 19% from 11%. Thus, TFBSA-modified flexible devices not only show much improved conversion

efficiency but also reveal superior bendability and self-healing nature. This work demonstrates a profound significance for commercialization of FPSCs with excellent bending resistance and self-healing properties.

Supporting Information

Supporting Information is available from the Wiley Online Library or from the author.

Declaration of Competing Interest

We declare that we have no financial and personal relationships with other people or organizations that can inappropriately influence our work, there is no professional or other personal interest of any nature or kind in any product, service and/or company that could be construed as influencing the position presented in, or the review of, the manuscript entitled.

Data availability

Data will be made available on request.

Acknowledgements

This work was supported by the Nature Science Funds of Sichuan Province (No. 2022NSFSC0266), the Youth Science and Technology Innovation Team Project of SWPU (No. 2019CXTD04), the Scientific Research Starting Project of SWPU (No. 2019QHZ013), and the Young Scholars Development Fund of SWPU (No. 201999010017).

Appendix A. Supporting information

Supplementary data associated with this article can be found in the online version at doi:10.1016/j.jallcom.2023.172427.

References

- [1] H. Min, D.Y. Lee, J. Kim, G. Kim, K.S. Lee, J. Kim, M.J. Paik, Y.K. Kim, K.S. Kim, M.G. Kim, T.J. Shin, S. Il Seok, Perovskite solar cells with atomically coherent interlayers on SnO₂ electrodes, *Nature* 598 (2021) 444–450, <https://doi.org/10.1038/s41586-021-03964-8>.
- [2] L. Yang, J. Feng, Z. Liu, Y. Duan, S. Zhan, S. Yang, K. He, Y. Li, Y. Zhou, N. Yuan, Record-efficiency flexible perovskite solar cells enabled by multifunctional organic ions interface passivation, *Adv. Mater.* (2022) 2201681, <https://doi.org/10.1002/adma.202201681>.
- [3] Z. Dai, S.K. Yadavalli, M. Hu, M. Chen, Y. Zhou, N.P. Padture, Effect of grain size on the fracture behavior of organic-inorganic halide perovskite thin films for solar

- cells, *Scr. Mater.* 185 (2020) 47–50, <https://doi.org/10.1016/j.scriptamat.2020.03.044>.
- [4] C. Ramirez, S.K. Yadavalli, H.F. Garces, Y. Zhou, N.P. Padture, Thermo-mechanical behavior of organic-inorganic halide perovskites for solar cells, *Scr. Mater.* 150 (2018) 36–41, <https://doi.org/10.1016/j.scriptamat.2018.02.022>.
- [5] S. Kim, H.S. Lee, J.M. Kim, S.W. Seo, J.H. Kim, C.W. Jang, S.-H. Choi, Effect of layer number on flexible perovskite solar cells employing multiple layers of graphene as transparent conductive electrodes, *J. Alloy. Compd.* 744 (2018) 404–411, <https://doi.org/10.1016/j.jallcom.2018.02.136>.
- [6] Z. Dai, S.K. Yadavalli, M. Chen, A. Abbaspourtajani, Y. Qi, N.P. Padture, Interfacial toughening with self-assembled monolayers enhances perovskite solar cell reliability, *Science* 372 (2021) 618–622, <https://doi.org/10.1126/science.abf5602>.
- [7] Z. Li, Z. Wang, C. Jia, Z. Wan, C. Zhi, C. Li, M. Zhang, C. Zhang, Z. Li, Annealing free tin oxide electron transport layers for flexible perovskite solar cells, *Nano Energy* 94 (2022), 106919, <https://doi.org/10.1016/j.nanoen.2022.106919>.
- [8] M.M. Tavakoli, K.-H. Tsui, Q. Zhang, J. He, Y. Yao, D. Li, Z. Fan, Highly efficient flexible perovskite solar cells with antireflection and self-cleaning nanostructures, *ACS Nano* 9 (2015) 10287–10295, <https://doi.org/10.1021/acsnano.5b04284>.
- [9] H. Chen, Two-step sequential deposition of organometal halide perovskite for photovoltaic application, *Adv. Funct. Mater.* 27 (2017) 1605654, <https://doi.org/10.1002/adfm.201605654>.
- [10] M. Kim, G.-H. Kim, T.K. Lee, I.W. Choi, H.W. Choi, Y. Jo, Y.J. Yoon, J.W. Kim, J. Lee, D. Huh, Methylammonium chloride induces intermediate phase stabilization for efficient perovskite solar cells, *Joule* 3 (2019) 2179–2192, <https://doi.org/10.1016/j.joule.2019.06.014>.
- [11] H.X. Dang, K. Wang, M. Ghasemi, M.-C. Tang, M. De Bastiani, E. Aydin, E. Dauzon, D. Barrit, J. Peng, D.-M. Smilgies, Multi-cation synergy suppresses phase segregation in mixed-halide perovskites, *Joule* 3 (2019) 1746–1764, <https://doi.org/10.1016/j.joule.2019.05.016>.
- [12] C. Wang, L. Guan, D. Zhao, Y. Yu, C.R. Grice, Z. Song, R.A. Awni, J. Chen, J. Wang, X. Zhao, Water vapor treatment of low-temperature deposited SnO_2 electron selective layers for efficient flexible perovskite solar cells, *ACS Energy Lett.* 2 (2017) 2118–2124, <https://doi.org/10.1021/acsenergylett.7b00644>.
- [13] M. Karimipour, S. Khazraei, B.J. Kim, G. Boschloo, E.M.J. Johansson, Efficient and bending durable flexible perovskite solar cells via interface modification using a combination of thin MoS_2 nanosheets and molecules binding to the perovskite, *Nano Energy* 95 (2022), 107044, <https://doi.org/10.1016/j.nanoen.2022.107044>.
- [14] Z. Huang, X. Hu, C. Liu, L. Tan, Y. Chen, Nucleation and crystallization control via polyurethane to enhance the bendability of perovskite solar cells with excellent device performance, *Adv. Funct. Mater.* 27 (2017) 1703061, <https://doi.org/10.1002/adfm.201703061>.
- [15] Y. Yu, F. Zhang, H. Yu, Self-healing perovskite solar cells, *Sol. Energy* 209 (2020) 408–414, <https://doi.org/10.1016/j.solener.2020.09.018>.
- [16] B.P. Finkenauer, Ma, K. Akriti, L. Dou, Degradation and self-healing in perovskite solar cells, *ACS Appl. Mater. Interfaces* 14 (2022) 24073–24088, <https://doi.org/10.1021/acsmi.2c01925>.
- [17] Y. Zhao, J. Wei, H. Li, Y. Yan, W. Zhou, D. Yu, Q. Zhao, A polymer scaffold for self-healing perovskite solar cells, *Nat. Commun.* 7 (2016) 10228, <https://doi.org/10.1038/ncomms10228>.
- [18] Y. Lan, Y. Wang, Y. Lai, Z. Cai, M. Tao, Y. Wang, M. Li, X. Dong, Y. Song, Thermally driven self-healing efficient flexible perovskite solar cells, *Nano Energy* 100 (2022), 107523, <https://doi.org/10.1016/j.nanoen.2022.107523>.
- [19] P. Zardari, A. Rostami, H. Shekaari, p-Phenylenediaminium iodide enabled self-healing perovskite solar cell, *Sci. Rep.* 10 (2020) 20011, <https://doi.org/10.1038/s41598-020-76365-y>.
- [20] Y. Lao, S. Yang, W. Yu, H. Guo, Y. Zou, Z. Chen, L. Xiao, Multifunctional π -conjugated additives for halide perovskite, *Adv. Sci.* 9 (2022) 2105307, <https://doi.org/10.1002/advs.202105307>.
- [21] Y. Dong, W. Shen, W. Dong, C. Bai, J. Zhao, Y. Zhou, F. Huang, Y.-B. Cheng, J. Zhong, Chlorobenzenesulfonic potassium salts as the efficient multifunctional passivator for the buried interface in regular perovskite solar cells, *Adv. Energy Mater.* 12 (2022) 2200417, <https://doi.org/10.1002/aenm.202200417>.
- [22] Y. Zou, W. Yu, Z. Tang, X. Li, H. Guo, G. Liu, Q. Zhang, Y. Zhang, Z. Zhang, C. Wu, J. Xiao, B. Qu, Z. Chen, L. Xiao, Improving interfacial charge transfer by multi-functional additive for high-performance carbon-based perovskite solar cells, *Appl. Phys. Lett.* 119 (2021), 151104, <https://doi.org/10.1063/5.0061869>.
- [23] K. Choi, J. Lee, H.I. Kim, C.W. Park, G.-W. Kim, H. Choi, S. Park, S.A. Park, T. Park, Thermally stable, planar hybrid perovskite solar cells with high efficiency, *Energy Environ. Sci.* 11 (2018) 3238–3247, <https://doi.org/10.1039/cbe02242a>.
- [24] X. Li, C.C. Chen, M. Cai, X. Hua, F. Xie, X. Liu, J. Hua, Y.T. Long, H. Tian, L. Han, Efficient passivation of hybrid perovskite solar cells using organic dyes with -COOH functional group, *Adv. Energy Mater.* 8 (2018) 1800715, <https://doi.org/10.1002/aenm.201800715>.
- [25] Li, C., anion immobilization through chemical bonding enhancement with fluorides for stable halide perovskite solar cells, *Nat. Energy*, 408. <https://doi.org/10.1038/s41560-019-0382-6>.
- [26] X. Gong, H. Li, R. Zhou, X. Peng, Y. Ouyang, H. Luo, X. Liu, J. Zhuang, H. Wang, Y. Ni, Strong electron acceptor of a fluorine-containing group leads to high performance of perovskite solar cells, *ACS Appl. Mater. Interfaces* 13 (2021) 41149–41158, <https://doi.org/10.1021/acsmi.1c07610>.
- [27] C. Zuo, L. Ding, Drop-casting to make efficient perovskite solar cells under high humidity, *Angew. Chem.* 133 (2021) 11342–11346, <https://doi.org/10.1002/anie.202101868>.
- [28] B. Liu, H. Bi, D. He, L. Bai, W. Wang, H. Yuan, Q. Song, P. Su, Z. Zang, T. Zhou, J. Chen, Interfacial defect passivation and stress release via multi-active-site ligand anchoring enables efficient and stable methylammonium-free perovskite solar cells, *ACS Energy Lett.* 6 (2021) 2526–2538, <https://doi.org/10.1021/acsenergylett.1c00794>.
- [29] Q. Dong, Y. Fang, Y. Shao, P. Mulligan, J. Qiu, L. Cao, J. Huang, Electron-hole diffusion lengths > 175 μm in solution-grown $\text{CH}_3\text{NH}_3\text{PbI}_3$ single crystals, *Science* 347 (2015) 967–970, <https://doi.org/10.1126/science.aaa5760>.
- [30] C.W. Jang, D.H. Shin, S.-H. Choi, Photostable electron-transport-layer-free flexible graphene quantum dots/perovskite solar cells by employing bathocuproine interlayer, *J. Alloy. Compd.* 886 (2021), 161355, <https://doi.org/10.1016/j.jallcom.2021.161355>.
- [31] N. Faraji, C. Qin, T. Matsushima, C. Adachi, J. Seidel, Grain boundary engineering of halide perovskite $\text{CH}_3\text{NH}_3\text{PbI}_3$ solar cells with photochemically active additives, *J. Phys. Chem. C* 122 (2018) 4817–4821, <https://doi.org/10.1021/acs.jpcc.8b00804>.
- [32] Y. Wen, Y.-G. Tang, G.-Q. Yan, Large grain size $\text{CH}_3\text{NH}_3\text{PbI}_3$ film for perovskite solar cells with hydroic acid additive, *AIP Adv.* 8 (2018), 095226, <https://doi.org/10.1063/1.5048424>.
- [33] R. Zhou, X. Liu, H. Li, H. Wang, Y. Ouyang, X. Gong, X. Peng, H. Luo, Y. Ni, W. Zou, Sulfonyl and carbonyl groups in MSTC effectively improve the performance and stability of perovskite solar cells, *Sol. RRL* (2021) 2100731, <https://doi.org/10.1002/solr.202100731>.
- [34] Y. Cui, C. Chen, C. Li, L. Chen, S.S. Bista, X. Liu, Y. Li, R.A. Awni, Z. Song, Y. Yan, Correlating hysteresis and stability with organic cation composition in the two-step solution-processed perovskite solar cells, *ACS Appl. Mater. Interfaces* 12 (2020) 10588–10596, <https://doi.org/10.1021/acsmi.9b23374>.
- [35] Y. Guo, J. Ma, H. Lei, F. Yao, B. Li, L. Xiong, G. Fang, Enhanced performance of perovskite solar cells via anti-solvent nonfullerene Lewis base IT-4F induced trap-passivation, *J. Mater. Chem. A* 6 (2018) 5919–5925, <https://doi.org/10.1039/c8ta00583d>.
- [36] Y. Lei, H. Li, X. Liu, C. Qiu, H. Wang, X. Gong, Y. Ni, R. Feng, J. Peng, Y. Liu, H. Li, Hydrogen-iodide bonding between glycine and perovskite greatly improve moisture stability for binary PSCs, *Org. Electron.* 108 (2022), 106573, <https://doi.org/10.1016/j.orgel.2022.106573>.
- [37] H.Y. Wang, W.J. Zou, Y.K. Ouyang, H. Luo, X.C. Liu, H.M. Li, Y. Lei, Y.F. Ni, Y. Fu, D. Zheng, Inducing crystal-oriented growth while inhibiting grain boundary migration with multifunctional ionic liquid for high-efficiency perovskite solar cells, *J. Alloy. Compd.* 929 (2022) 7, <https://doi.org/10.1016/j.jallcom.2022.167051>.
- [38] W. Nie, J.-C. Blanc, A.J. Neukirch, K. Appavoo, H. Tsai, M. Chhowalla, M. A. Alam, M.Y. Sfeir, C. Katan, J. Even, Light-activated photocurrent degradation and self-healing in perovskite solar cells, *Nat. Commun.* 7 (2016) 1–9, <https://doi.org/10.1038/ncomms11574>.
- [39] Y. Lei, H. Li, X. Liu, H. Wang, Y. Ni, X. Gong, W. Zou, Y. Tang, S. Liu, Enhanced bending resistance and efficiency of flexible pscs derived from self-healing and passivation double function of a silane coupling agent, *Adv. Mater. Interfaces* 9 (2022) 2200992, <https://doi.org/10.1002/admi.202200992>.
- [40] C. Ding, Y. Zhang, F. Liu, Y. Kitabatake, S. Hayase, T. Toyoda, K. Yoshino, T. Minemoto, K. Katayama, Q. Shen, Effect of the conduction band offset on interfacial recombination behavior of the planar perovskite solar cells, *Nano Energy* 53 (2018) 17–26, <https://doi.org/10.1016/j.nanoen.2018.08.031>.
- [41] H. Xie, T. Liang, X. Yin, J. Liu, D. Liu, G. Wang, B. Gao, W. Que, Mechanical stability study on PEDOT:PSS-based ITO-free flexible perovskite solar cells, *ACS Appl. Energ. Mater.* 5 (2022) 3081–3091, <https://doi.org/10.1021/acsaem.1c03696>.
- [42] J. Dong, J. Jia, X. Feng, B. Shi, Y. Wu, Y. Zhang, J. Wu, B. Cao, Ligand exchange of SnO_2 effectively improving the efficiency of flexible perovskite solar cells, *J. Alloy. Compd.* 883 (2021), 160827, <https://doi.org/10.1016/j.jallcom.2021.160827>.
- [43] M. Li, Y.-G. Yang, Z.-K. Wang, T. Kang, Q. Wang, S.-H. Turren-Cruz, X.-Y. Gao, C.-S. Hsu, L.-S. Liao, A. Abate, Perovskite grains embraced in a soft fullerene network make highly efficient flexible solar cells with superior mechanical stability, *Adv. Mater.* 31 (2019) 1901519, <https://doi.org/10.1002/adma.201901519>.
- [44] D.H. Jung, Y.J. Oh, Y.S. Nam, H. Lee, Effect of layer number on the properties of stable and flexible perovskite solar cells using two dimensional material, *J. Alloy. Compd.* 850 (2021), 156752, <https://doi.org/10.1016/j.jallcom.2020.156752>.
- [45] H. Sun, P. Dai, X. Li, J. Ning, S. Wang, Y. Qi, Strategies and methods for fabricating high quality metal halide perovskite thin films for solar cells, *J. Energy Chem.* 60 (2021) 300–333, <https://doi.org/10.1016/j.jechem.2021.01.001>.